Thermodynamics of the OWC chamber: Experimental turbine performance under stationary flow

Thermodynamics of the OWC chamber: experimental turbine performance under stationary flow.

A. Moñino[a], C. Quirós[a], F. Mengíbar[a], E. Medina-Lopez[a,b], M. Clavero[a]

[a] *Andalusian Institute for Earth System Research, University of Granada. Av. del Mediterráneo s/n. 18006, Granada (Spain)*
[b] *Institute for Infrastructure and Environment. School of Engineering. University of Edinburgh. The King's Buildings, EH9 3JL Edinburgh (United Kingdom)*

Abstract

Among the different devices designed to extract energy from waves, the Oscillating Water Column (OWC) operating an air turbine has been one of the most studied in recent years. The aim of this paper is to study the polytropic exponent associated to the thermodynamic process that takes place through the turbine in a non-idealised environment. A real gas model is applied, considering the influence of the moisture in the air chamber. Experimental data from a simplified OWC chamber set up under stationary flow are interpreted within the frame of an analytical real gas model. For that purpose, thermodynamic variables involved in the compression/expansion process have been calculated with the implementation of a real gas model. Following the results, in which differences between the ideal gas adiabatic polytropic process and the real gas model are observed, a new value for the polytropic exponent is proposed, representing a non–adiabatic real gas behaviour for the air–water vapour mixture. This approach allows a fine adjustment prediction of OWC performance, that can result more realistic in the case of OWC performance prediction under moderate wave climate conditions. From that on, new management guidelines can be developed, in which eventually moderate/low production prospects can be counterbalanced with more efficient and low–cost design.

Keywords: Experimental, Oscillating Water Column (OWC), Polytropic index, Real gas, Wave Energy Converter (WEC), Wind Tunnel

Email address: christianquirosnebrera@gmail.com (C. Quirós)

1. Introduction

Energy, one of the most important factors involved in countries economy growth, supporting a significant percentage of Gross Domestic Product, driver for productivity and necessary component for any day-to-day activity, but on the contrary, its production turn out being one of the main agent of global environmental damage [1, 2].

Nowadays, despite fossil resources usage remains significant, the current global energy outlook suggest that renewable alternatives progressively gain importance. In Europe this trend is noticeable reaching a $34,2\%$ of renewable-based electricity production [3].

Inside the context of alternative energy resources, ocean energy appears as a potential resource whose exploitation begins to be a reality throughout the last years. Currently, there are many technologies developed for its use. Conceived as single devices or arrays, a number of those energy converters are still prototypes in experimental phase. Exceptionally, some few devices have been full-scale built ([4, 5]). However, wave resource prospective for the forthcoming decades reaches up to 26MW in Europe, out of 170MW worldwide (see e.g. Refs. [6]-[9]).

Among the designs developed for sea power extraction, [10]-[12], one of the most widely studied is the Oscillating Water Column device (hereinafter *OWC*), [13]. This wave energy converter (hereinafter *WEC*) essentially consists of a partially submerged air cavity opened to the sea at the bottom. The free surface oscillation forced by the incident waves alternately compresses and expands the air volume confined inside it, setting off the rotation of a turbine –usually consisting of a Wells type one– used as power take off system (*PTO*), [14, 15].

The main advantage of the OWC device compared to other *WECs* lies on its simplicity, since the only moving part in the PTO is the turbine. In terms of OWC development around key aspects involved in the device management, there are different lines of work: analysis of the mutual influence between device and the surroundings ([15]-[19]), geometrical control and optimization ([20]-[24]), physical operational parameters ([25]-[27]), numerical modeling ([28]-[31]), time-size scaling of forcing agents and spatial optimization ([32, 33]), device reliability, profitability and social impact ([34]-[36]), among others.

An appropriate characterization of processes and agents involved in the OWC performance leads to the development of tools for management, in which an accurate apporach to the *PTO* expected performance is implemented. Starting from the classic theoretical formulation, the OWC device physical behaviour is usually described according to the radiation–diffraction problem, [37, 38]. Different case studies are defined to match specific considerations regarding geometry and location ([15], [39, 40]), spatial arrangement of device arrays ([41]), device interaction with the coast line geometry ([16, 42]), bedform influence on the device response ([18, 43]).

Concerning the compression–expansion process in the OWC operation, previous literature accept in a generalized way the underlying thermodynamic process as the adiabatic cycle of an ideal gas. Therefore, theoretical formulation and conceptual simplifications are assumed. Even if atmospheric conditions such as ambient moisture or other thermodynamic variables are usually not accounted for, some authors have advanced in implementing the thermodynamic focusing on the OWC theory ([21, 44]). However, a deeper consideration of the working fluid as a real gas in which humidity, temperature and pressure effects are taken into account, might lead to deviations in its behaviour with respect to the theoretical ideal gas.

Currently, the influence of a working fluid consisting of a mixture of air and another gas phase on turbine efficiency (either vapour of water or some kind of fuel) has been widely studied and is of common application in the field of gas turbines in thermal power plants ([45]-[48]). On the other hand, models developed to quantify humidity effects on gas turbines, have been adjusted to processes where the working fluid is related to higher temperature and pressure states than those presented in OWC devices, so new considerations might be required for the purpose ([47, 48]).

In recent years, the thermodynamic process through an OWC chamber model has been object of study ([49]-[51]). That research focuses on the deviation related with real gas model as compared to the ideal gas. The real gas model modifies the ideal gas behaviour by means of Virial Expansion equations, [52], also modifying the description of the polytropic process equation. In fact, research has been devoted to the the polytropic processes in real gases in terms of Virial expansion coefficients ([53]-[56]). Studies conclude that performance variations are linked to temperature and humidity factors in the working fluid. In the case of a mixture of dry air and water vapour, such as the OWC conditions, the thermodynamic process of compression–expansion and the reduction in pressure drop and pneumatic power are better explained under the hypothesis of real gas system. In addition, the process does not present a purely adiabatic behaviour, even if the real gas condition is added.

One important point related with the previous facts, specially when dealing with results deduced from model test to be extended to prototypes, is the scale effects in the air flow, hence related with the thermodynamic processes as described above. Those scale effects have been deeply researched by some authors ([57]) and provide with a methodology for fine adjustment and generalization of the results of model studies on OWC chambers, once the Thermodynamics of the cycle process is clearly assessed.

The objective of this paper is to analyze the nature of the polytropic compression/expansion process of the real gas system (air-water vapour) inside the OWC chamber, to identify the conditions under which the thermodynamic process takes place in terms of the polytropic process equation, and to determinate the polytropic exponent that defines the process.

This paper is organized as follows: first, the thermodynamic background supporting the real gas model and its applicability to the OWC air chamber thermodynamic process is presented. Afterwards, a description of the experimental set up used to test the real gas model hypothesis is carried out. Finally, results and discussion are exposed, followed by the conclusions and future research sections.

2. Thermodynamic background

2.1. Process in a simple closed system

In order to appropriately implement the basic principles concerning the thermodynamic process of air compression and expansion inside the OWC chamber and following the research line traced by the authors in [49, 50], a gas system enclosed in a moving and deformable control volume is considered, see figure 1.

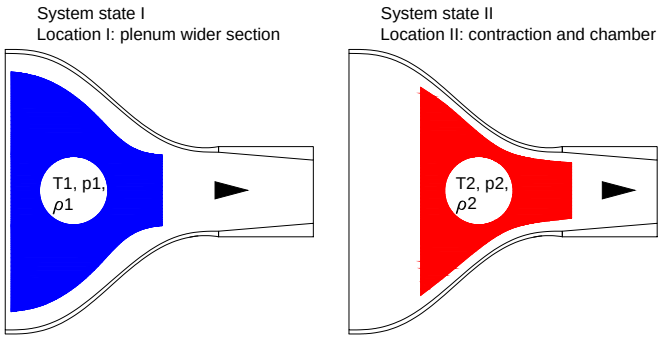

Figure 1: Control Volume deformation of the thermodynamic system flowing through the set up. System state I & location I (left). System state II & location II (right).

The situation described in figure 1 might as well represent the process of an air flow being compressed inside an OWC chamber, where the turbine would be mounted at the right end. Hence, under the *Lagrangian* standpoint of the Control Volume established, the thermodynamic properties of the air both in the inflow and outflow sections can be related through a process equation.

In the case of a polytropic process of a simple closed system, the process equation is defined as:

$$p v_m^n = const \tag{1}$$

where p is the thermodynamic pressure, $v_m = V/N$ is the molar volume of the gas enclosed in the control volume, and n is the polytropic exponent, which takes an specific value depending on both the type of process and the nature of the system (for example an adiabatic process of an ideal gas takes $n \equiv \gamma = 5/3$, while for dry air it takes $n = 1.4$).

The process equation (1) represents a relationship between thermodynamic variables $(T_1, p_1, v_{m\,1})$ and $(T_2, p_2,\ v_{m\,2})$ describing the system state both prior and after compression. Therefore, the process comprises a sequence of intermediate states represented by a curve in the $p - V$ thermodynamic space —figure 2— rather than by a system displacement in the coordinate space. In fact, what actually happens is that the system state evolves between the initial and final conditions which, in turn, correspond to different locations.

More specifically in the case of an OWC chamber, let us consider an observer in a reference frame moving with the closed gas system represented in figure 1. From the observer's reference a compression process takes place in the simple closed system with related changes in the state variables (T, p, v_m), the nature of them depending on how the system exchanges heat and temperature with the medium. Hence, at the end of that compression process —when the control volume reaches the turbine and flows through it— a new state is reached, which is related to the initial state prior to compression through a process as described by the polytropic equation (1) and represented in figure 2. Indeed, the fact that the new system state corresponds to a location different to the initial one is essentially irrelevant, given both the system is closed —therefore there has been not mass exchange in the moving control volume— and the flow is stationary. The process would have been the same if a static deformable control volume inside a piston would have been considered,

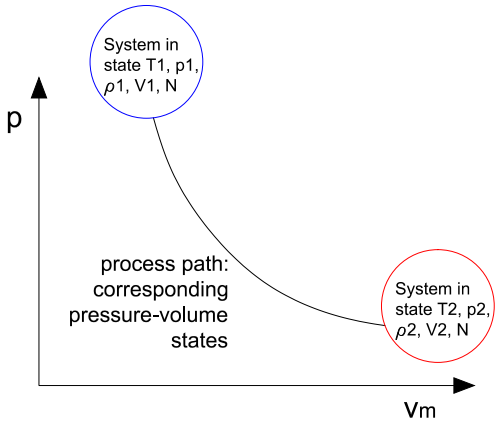

Figure 2: System process in the $p-V$ thermodynamic space.

in which the compression would have taken place by the piston action and under the same heat/temperature exchange conditions. In conclusion, when dealing with variations of system state variables between two points in a flow field such as the example represented in figure 1, actually the thermodynamic formalism is applied between two equilibrium states in the $p-V$ space connected by a process equation, even if those two states correspond to system conditions that are located at different points in the coordinate space.

2.2. Theoretical formulation

The Thermodynamics formalism can be applied to relate the initial state of the system in the contraction region with its final state downwind the OWC chamber and turbine. The following rationale and its conclusions have been applied and validated by the authors in previous research, [50].

Let us suppose a system evolving from $(T_1, p_1, v_{m\,1})$ to $(T_2, p_2, v_{m\,2})$ according to a process in which a certain state variable y remains constant. A specific heat under constant y can be defined, as the thermodynamic variable representing the amount of heat required for that process to occur under those conditions, [58], say:

$$C_y = T\left(\frac{\partial s}{\partial T}\right)_y \tag{2}$$

where $s = S/N$ is the unitary entropy. If the variable y represents pressure or volume, then the expression (2) leads to the definitions of the well known specific heats under constant pressure and volume, C_p and C_V respectively:

$$\begin{aligned} C_p &= T\left(\frac{\partial s}{\partial T}\right)_p \\ C_V &= T\left(\frac{\partial s}{\partial T}\right)_{v_m} \end{aligned} \tag{3}$$

The polytropic index m can also be defined for future use in the form:

$$m = \frac{C_y - C_p}{C_y - C_V} \tag{4}$$

so relating the specific heat C_y with the specific heats C_p and C_V. Once defined C_y and m, a differential equation between state variables p and V can be deduced to find an expression of n. For this purpose, the first step is to set the differential form of the entropy both in terms of (T, p) and (T, v_m):

$$\begin{aligned} ds &= \left(\frac{\partial s}{\partial T}\right)_p dT + \left(\frac{\partial s}{\partial p}\right)_T dp \\ ds &= \left(\frac{\partial s}{\partial T}\right)_{v_m} dT + \left(\frac{\partial s}{\partial v_m}\right)_T dv_m \end{aligned} \tag{5}$$

Assuming the variation in temperature between the initial and final states, the change in entropy in the process under constant y is therefore:

$$\begin{aligned}\left(\frac{\partial s}{\partial T}\right)_y &= \left(\frac{\partial s}{\partial T}\right)_p + \left(\frac{\partial s}{\partial p}\right)_T \left(\frac{\partial p}{\partial T}\right)_y \\ \left(\frac{\partial s}{\partial T}\right)_y &= \left(\frac{\partial s}{\partial T}\right)_{v_m} + \left(\frac{\partial s}{\partial v_m}\right)_T \left(\frac{\partial v_m}{\partial T}\right)_y\end{aligned} \tag{6}$$

The derivatives of entropy with respect to p and v_m can be expressed in a more convenient form in terms of the isobaric expansion coefficient α and the isothermal compressibility coefficient k_T, [58]:

$$\begin{aligned}\left(\frac{\partial s}{\partial p}\right)_T &= -\left(\frac{\partial v_m}{\partial T}\right)_p = -v_m\alpha \\ \left(\frac{\partial s}{\partial v_m}\right)_T &= \left(\frac{\partial s}{\partial p}\right)_T \left(\frac{\partial p}{\partial v_m}\right)_T = -\left(\frac{\partial v_m}{\partial T}\right)_p \left(\frac{\partial p}{\partial v_m}\right)_T = \frac{\alpha}{k_T}\end{aligned} \tag{7}$$

with:

$$\alpha = \frac{1}{V}\left(\frac{\partial V}{\partial T}\right)_{p,N} \tag{8}$$

and:

$$k_T = -\frac{1}{V}\left(\frac{\partial V}{\partial p}\right)_{T,N} \tag{9}$$

Combining the definitions (3) of C_p and C_V along with (2) and (7), in (6):

$$\begin{aligned}C_y - C_p &= -Tv_m\alpha\left(\frac{\partial p}{\partial T}\right)_y \\ C_y - C_p &= \frac{T\alpha}{k_T}\left(\frac{\partial v_m}{\partial T}\right)_y\end{aligned} \tag{10}$$

If both expressions are taken to the form of a division and the definition (4) of the index m is used, a differential equation for the process is deduced:

$$\left(\frac{\partial p}{\partial v_m}\right)_y = -\frac{m}{v_m k_T} \tag{11}$$

The solution of (11) provides a functional relationship between state variables p and v, for a general process of a simple closed system in which the system variable y is held constant with no additional restrictions. Getting back now to the polytropic process defined by (1) and expressing it in its differential form:

$$v_m^n dp + n v_m^{n-1} p dv_m = 0 \tag{12}$$

and differentiating v_m with respect to p for $y = const$:

$$\left(\frac{\partial v_m}{\partial p}\right)_y = -\frac{v_m}{np} \tag{13}$$

it is feasible to compare the general process equation (1) with the differential equation (12) for the polytropic system, so the expression for the polytropic index is finally deduced:

$$n = \frac{m}{pk_T} \tag{14}$$

The expression (14) is yet unsolved unless the nature of the system and the type of process undergone by it are known. For example, in the case of an adiabatic process in a simple closed system it is found that the entropy is constant, so $y \equiv s$ and:

$$m = C_p/C_V \equiv \gamma \tag{15}$$

where γ represents the adiabatic exponent.

Simultaneously, in the case of an ideal gas the thermal equation of state reads:

$$pv_m = R_0 T \tag{16}$$

so it is found from (9) that $k_T = 1/p$ and:

$$n = m \tag{17}$$

Finally, an adiabatic process of an ideal gas is represented by:

$$n = m = \gamma \tag{18}$$

and so the polytropic exponent and the polytropic index are equal to the adiabatic coefficient γ. More specifically, for an ideal monoatomic gas system it is $C_p = 5/2R_0$ and $C_V = 3/2R_0$, [58], and in consequence for an adiabatic process it is deduced $n = \gamma = C_p/C_V \simeq 1.67$. In the case of air treated as an ideal system, it is found $n = \gamma = C_p/C_V \simeq 1.4$ for an adiabatic process, [59]. On the other hand, if the process is isothermal, following the previous rationale and accounting for the fact that now it is $y \equiv T$, it is found $m = 1$, and $n = 1$ in the case of an ideal system. In any case, those rules might not always apply for other systems and/or conditions, as it will be discussed later.

2.3. Real gas process

Turning back now to the concerned problem of the OWC compression process, an explicit form expression of the exponent n allows a further implementation of the characteristics of the system and the nature of the process in the thermodynamic formulation of the OWC problem. In that framework, the working fluid is comprised by a mixture of dry air and water vapour with observed deviations from the ideal gas behaviour as outlined in [49]. Following the track started with that research, the goal now is to find an explicit form for the polytropic exponent n so that equation (1) contains all the required information to describe the complete sequence of states, focusing on the lagrangian approach to the compression process undergone by the simple closed system considered.

Indeed, when dealing with a real gas system the formulation is slightly modified in order to account for those differences. The thermal equation of state for a real gas can be expressed in the modified form:

$$pv_m = ZR_0 T \tag{19}$$

where the compressibility factor Z can be expressed in terms of the Virial expansion, [52]:

$$Z = \frac{pv_m}{R_0 T} \simeq 1 + \frac{B}{v_m} + \frac{C}{v_m^2} + \cdots \tag{20}$$

in which the so called second virial coefficient B is a function of temperature to be determined empirically. When the Thermodynamic formalism is applied to the deduced expression for the polytropic index (11) accounting for (20), n takes the form:

$$n = \frac{m}{1 - \dfrac{p}{Z}\left(\dfrac{\partial Z}{\partial p}\right)_T} \tag{21}$$

The compressibility factor Z can be expressed in a more convenient form by combining the expansion (20) and the equation of state (19):

$$Z = 1 + \frac{Bp_c}{R_0 T_c}\frac{p_r}{T_r} \tag{22}$$

in which p_c and T_c are the critical values of pressure and temperature for the gas. The critical temperature and its corresponding pressure value represent the state beyond which a gas cannot be liquified by compression, and they are

reference values used for calculations with reduced state variables T_r and p_r, so that $T_r = T/T_c$ and $p_r = p/p_c$. In the case of water $T_c = 647\,K$ and $p_c = 218\,atm = 220.89 \cdot 10^5\,Pa$. Therefore:

$$\left(\frac{\partial Z}{\partial p}\right)_T = \frac{B}{R_0 T} = \frac{B}{R_0 T_c}\frac{1}{T_r} \tag{23}$$

and:

$$\frac{p}{Z}\left(\frac{\partial Z}{\partial p}\right)_T = \frac{1}{Z}\frac{B p_c}{R_0 T_c}\frac{p_r}{T_r} \tag{24}$$

hence:

$$1 - \frac{p}{Z}\left(\frac{\partial Z}{\partial p}\right)_T = \frac{1}{Z}\left(Z - \frac{B p_c}{R_0 T_c}\frac{p_r}{T_r}\right) = \frac{1}{Z}\left(1 + \frac{B p_c}{R_0 T_c}\frac{p_r}{T_r} - \frac{B p_c}{R_0 T_c}\frac{p_r}{T_r}\right) = \frac{1}{Z} \tag{25}$$

Using the previous result in (21), a modified expression for the polytropic index n in an general process of a real gas is finally deduced:

$$n = Zm \tag{26}$$

where basically m stands for a general process according to (4) and Z is calculated from (22). In the case of an adiabatic process $m = C_p/C_V$ and:

$$n = Z\frac{C_p}{C_V} \tag{27}$$

It is clear from the above discussion on the index n that a deviation out of the expected values, e. g. $n = C_p/C_V = 1.67$ in the case of an adiabatic process of an ideal monoatomic system, would reveal either a system which is not entirely ideal and so $n \neq m$, or a process which is no totally adiabatic and so $m \neq C_p/C_V$, or most probably a combination of both.

The state variables involved in the calculations for the real gas are evaluated as corrections from the state variables for the ideal gas. Regarding the specific heats, C_p and C_V, and molar enthalpy h, the following expressions can be derived once the real gas formalism and virial expansion are considered —please refer to [58] for further details on the rationale—. Hence:

$$C_p = C_p^* + p\delta C_p = C_p^* - T\frac{d^2 B}{dT^2}p \tag{28}$$

and:

$$C_V = C_V^* + \delta C_V = C_V^* - \frac{R_0}{v_m}\frac{d}{dT}\left(T^2\frac{dB}{dT}\right) \tag{29}$$

for the specific heats, and:

$$h = h^* + p\delta h = h^* + Bp - T\frac{dB}{dT}p \tag{30}$$

for the unitary enthalpy, where the "*" stands for the ideal gas variables and B is the second virial coefficient. The unitary enthalpy of the ideal gas can be expressed as a function of the specific heat C_p^* and the flow velocity U in the considered section:

$$h^* = C_p^* T + \frac{1}{2}U^2 \tag{31}$$

The main issue is henceforth the calculation of B for a given state. As a first approach, the virial coefficient B can be determined applying the *Tsonopoulos* innovation, [60], which reads:

$$\frac{B p_c}{R_0 T_c} = f_0 + \omega f_1 + \chi_{mol} f_2 \tag{32}$$

where f_0, f_1 and f_2 are temperature correlation functions, ω is the acentric factor, χ_{mol} is the molar fraction of vapour in dry air. In the case of the air-water vapour mixture —e. g. the real gas enclosed in the OWC chamber— and assuming spherically–shaped molecules, it is $\omega \simeq 0$ and in consequence B is calculated form f_0 and f_2:

$$\begin{cases} f_0 = 0.1445 - \dfrac{0.330}{T_r} - \dfrac{0.1385}{T_r^2} - \dfrac{0,0121}{T_r^3} - \dfrac{0.000607}{T_r^8} \\ f_2 = \dfrac{0.0297}{T_r^6} - \dfrac{0.0229}{T_r^8} \end{cases} \tag{33}$$

A graphical representation of B can be observed in figure 3, according to both experimental data and correlations. Therefore, considering either the empirical expression (32) or the graphical representation in figure 3, the state functions of the real gas can be estimated from (28), (29) and (30). The methodology can also be applied in the reverse direction from (31), for example in the calculation of the required temperature change in a system process between two equilibrium states under the condition of the enthalpy conservation that can be solved from:

$$U_2 = \sqrt{2(h_1 - C_{p\,2} T_2 - \delta h p_2)} \tag{34}$$

once the enthalpy h_1 is known. In that case the methodology might result less precise for the lower range of temperature —say $T < 350\,K$, where the response of B is on the whole linear—, although it has provided conclusive results in terms of the important role of the deviations from the ideal gas performance. However, a further review of the values of B —and therefore of the values of n— to be applied for the standard system conditions to be observed in the OWC context, is required to advance in the identification of the nature of the compression/expansion process and in the air exchange through the turbine.

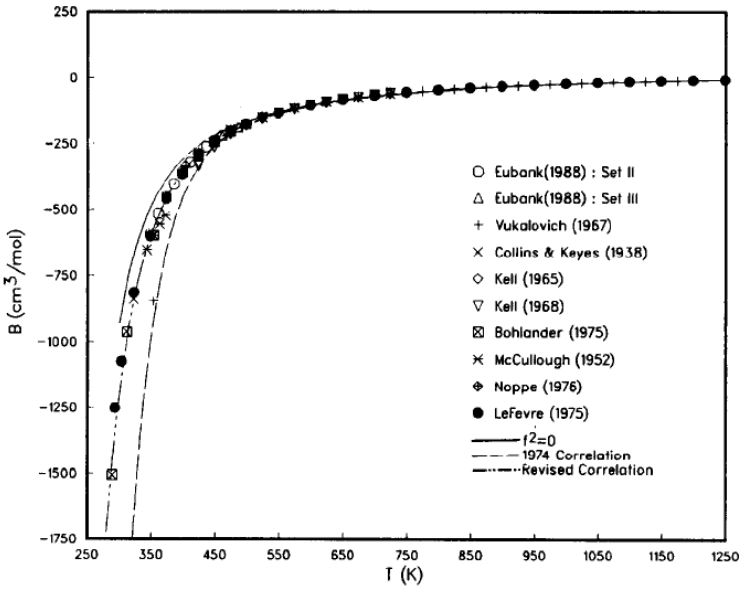

Figure 3: Second virial coefficient, B, [60]. The ordinary range of temperature for an OWC system falls under $350\,K$, corresponding to the leftmost region of the temperature axis.

3. Experimental set up

New tests are now conducted in a wind tunnel of the Andalusian Institute for Earth System Research (University of Granada). The test is focused on the thermodynamics of the flow compression through the OWC chamber and turbine. A new plenum is implemented for the improvement of the flow aerodynamics at the test section inlet.

The experimental framework consists of a methacrylate wind tunnel —see figure 4— with a $0.360\,m$ wide $\times\, 0.43\,m$ high characteristic section, and a wind speed capacity up to $20\,m/s$ generated by a $2.2\,kW$ electric turbine controlled through a frequency converter.

The test section has been improved with a plenum that ensures a smooth flow transition from the rectangular $0.36\,m \times 0.43\,m$ cross section to a $0.1\,m$ diameter circular section, at the end of which a convergent transition to the

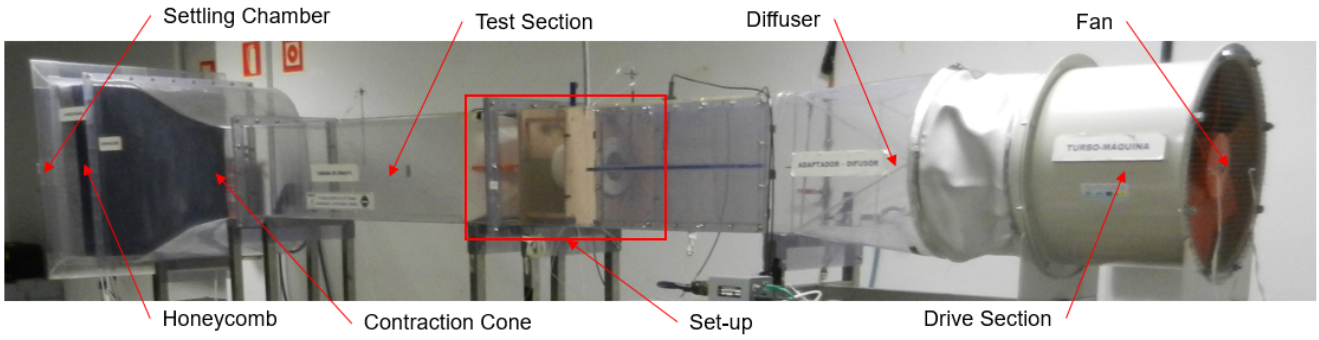

Figure 4: Wind tunnel set up.

$0.08\,m$ diameter OWC chamber is implemented —see figure 6 (left)—. The design of the plenum follows the guidelines proposed in [61], so that a balance is ensured between minimum contraction length and prevention of boundary layer separation along the concave/convex contour due to adverse pressure gradients. The plenum longitudinal section is sketched in figure 6 (right), following the geometrical definition given by the expression:

$$y(x) = H_i - (H_i - H_e)(6x'^5 - 15x'^4 + 10x'^3) \tag{35}$$

where y is the vertical coordinate, H_i and H_e are the heights of the opening at the inlet and exit sections measured from the center axis, and $x' = x/L$ is the horizontal coordinate normalized by the contraction length L.

The length–to–height ratio of the contraction is chosen so that $L/H_i = 1$, ensuring no boundary layer separation from figure 5 (white dots region). Under that condition the deviation of flow velocity from the center line value is approximately $0.8\,\%$. Deviations of velocity above that value might lead to boundary layer separation when reaching the threshold of $1.6\,\%$ as observed in figure 5 (upper and lower solid dots regions).

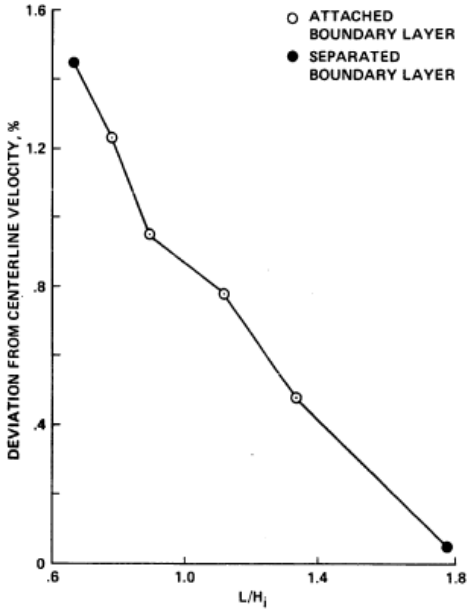

Figure 5: Velocity deviation from centerline values vs. L/H_i, [61].

Since the contraction represents the transition from a rectangular section to a circular one, the value of H_i to be chosen for the calculation of L depends on the choice of the representative dimension of the inlet section. For the contraction design it has been considered the diagonal measured from the corner of the rectangular inlet section to the center axis with $H_i = 0.27\,m$, see figure 6 (left). That way the maximum contraction length is attained according to $L = H_i = 0.27\,m$, and the coordinates of the generatrices starting from the corner vertices of the inlet section can be deduced from 35. Therefore, the generatrices corresponding to the vertical and horizontal sides correspond to values of

L/H_i greater than unit, so inducing a slight decrease in the deviation of the velocity along those boundaries with respect to the centre line according to figure 5, yet with no flow separation.

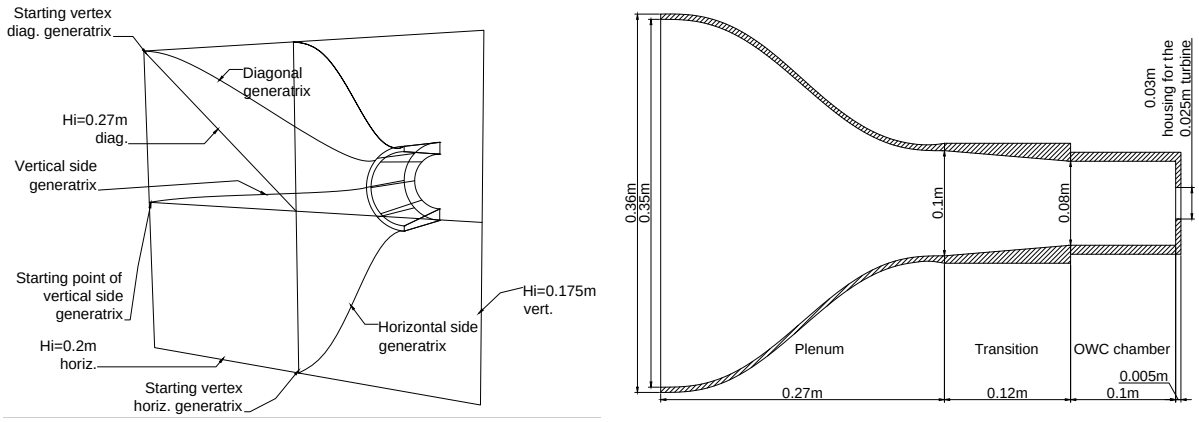

Figure 6: Plenum generatrix scheme (left) and set-up longitudinal section (right).

As it has been pointed out above, the OWC chamber consists of a $0.08\,m$ diameter cylindrical nylon shaft at the end of which the turbine is embedded, figure 7. The turbine characteristics are: diameter $D_t = 0.025\,m$, cross section area $A_t = 3.5906 \cdot 10^{-4}\,m^2$ (center to blade tip), blades area $A_b = 2.4271 \cdot 10^{-4}\,m^2$, and solidity $\sigma = 0.7315$.

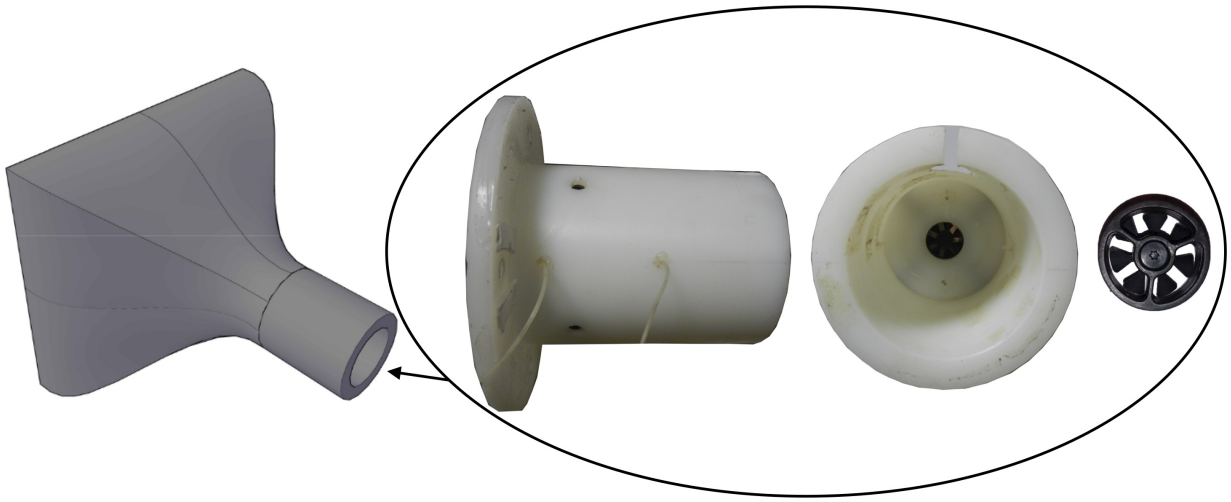

Figure 7: OWC turbine, OWC chamber and its relative position with respect to the plenum.

The turbine performance follows the calibration curve as presented in [49]. The rotor reveals a linear response between pressure jump and flow discharge, as represented in figure 8. Air velocity inside the $0.08\,m$ diameter OWC shaft has been considered for the calculation of the air volumetric discharge. For the considered range of values, the pressure drop Δp can be related with the turbine rotation speed N in *r.p.m.* through the linear expression:

$$\Delta p \simeq 98.4 \cdot 10^{-3} N - 126.1 \tag{36}$$

The expression (36) can be used to estimate a representative value of the pressure drop through the turbine once the turbine rotation N be measured. That would be the case, for example, in experiments conducted with the turbine shaft mounted on an OWC chamber to be tested under regular wave conditions in a wave basin,

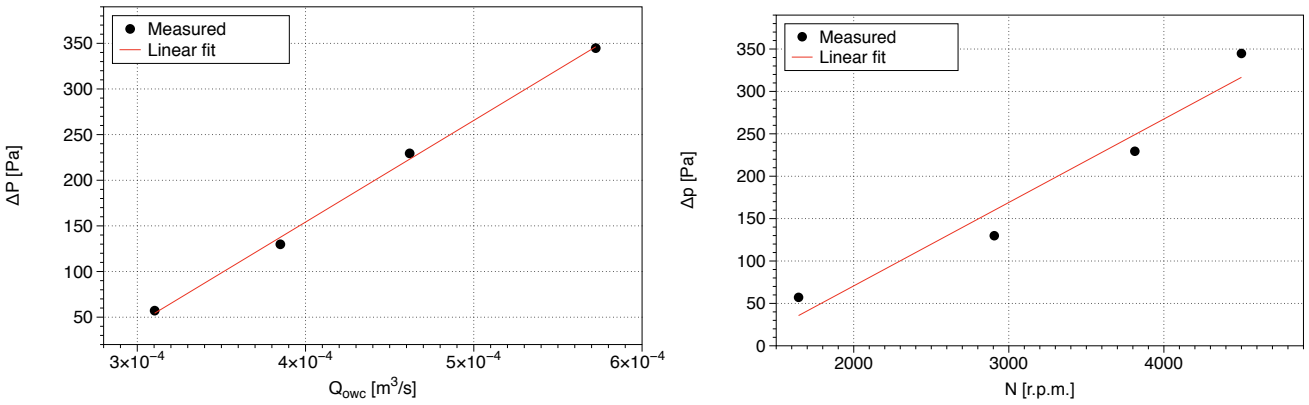

Figure 8: Pressure drop vs. air flow for the experimental set up (left) and pressure drop vs. turbine speed for the experimental set up (right).

Data of pressure, air velocity, temperature and moisture have been collected with pressure taps connected to a pressure transducer system, a hot wire, Pitot tube probes and temperature-moisture gauges, respectively, following the placement locations represented in figure 9 . A view of the main inlet and outlet gauges placement can be observed in figure 10.

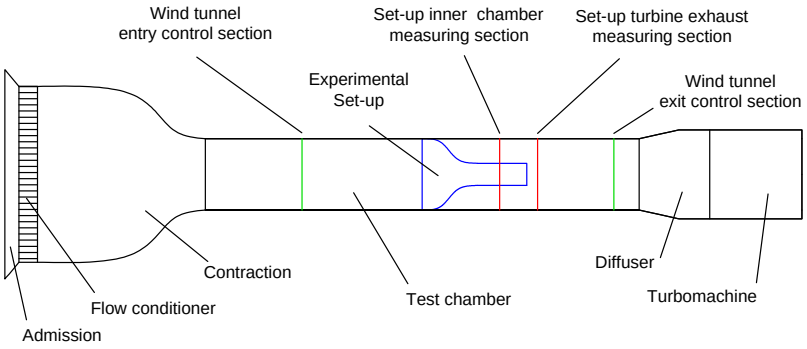

Figure 9: Schematic reference of gauges placement.

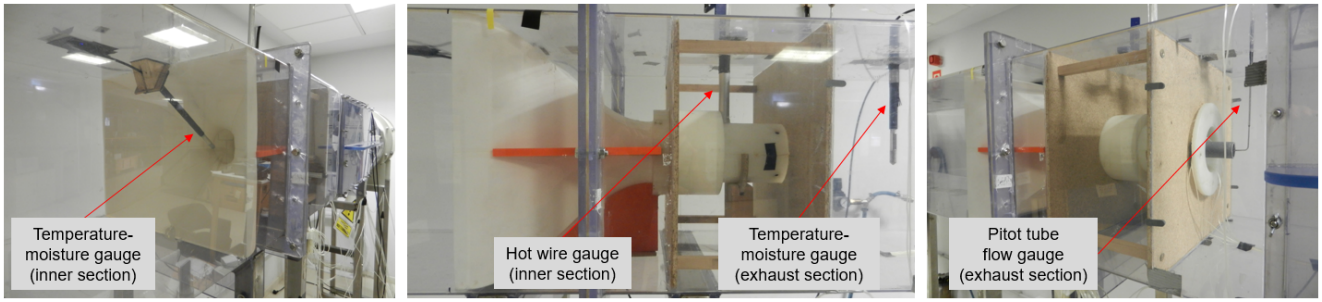

Figure 10: Detailed view of temperature–moisture, hot wire and pitot tube flow gauges.

Following the methodology described in [49], the static and total pressure distributions inside and outside the OWC chamber have been measured with pressure taps placed at specific locations in the nylon shaft as depicted in figure 11. A total of 14 taps connected to a *DTC Initium* pressure transducer system working at a sampling rate of 625 Hz has been used, four of them (two for static and two for total pressures) at the turbine intake, four others according to the same scheme for the outtake section and the rest have been used to ensure the flow uniformity throughout the set-up. On the other hand, the air velocity has been measured by means of a *TSI–IFA300* hot wire anemometer in the inflow section, whole for the outflow section a Pitot tube has been used. Finally, two *Vaisala HUMICAP HMT130*

temperature–humidity probes have been placed in the chamber plenum inlet section and in the wake region leeward the turbine.

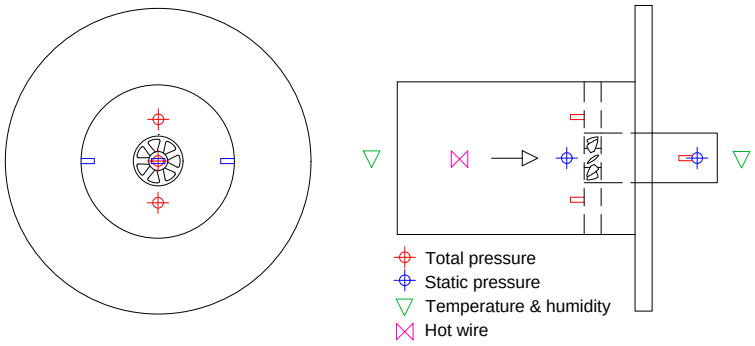

Figure 11: Pressure taps, temperature–humidity gauges and hot wire in the experimental set-up.

As it can be seen in the figure 11, the measurement systems are in all cases located close to the set up longitudinal axis. In the case of inlet gauges placement, they are sensibly more dispersed than at the outlet region due to the greater space limitation. We can list to downwind direction from the outtake plenum section to the intake turbine section a moisture-temperature gauge, a hot wire gauge and four pressure taps for the inlet measures, whereas for the outlet measures all the Pitot tube probe, four pressure taps and a second moisture-temperature gauge are located next to the outtake turbine section.

With all the previous configuration in mind, measured system variables are considered essentially uniform across the test sections. While some disturbances might be present due to the random nature of air flow –even if the wind tunnel set up ensures uniformity–, the bulk section values are considered enough representative of the system state following the concept depicted in figure 1.

4. Results and discussion

Experimental observations are analyzed and compared with the outcomes of the implementation of the real gas methodology. Strictly speaking in terms of the thermodynamic process, the state variables used to characterize the initial and final system states, eventually related with the conditions at two different locations –inside the camera and leeward side of the turbine–, correspond to a system state in which properties are statistically stationary. Hence the experimental conditions of stationary flow provide a framework for the correct interpretation of the results, without loss of generality when extended to the OWC oscillatory flow.

4.1. Temperature in the final state

Values of moisture, temperature and static and dynamic pressure have been measured as described in the experimental set up. Datasets of temperature and pressure have been considered for two moisture conditions, say relative humidities of 45 % and 70 %. From the empirically observed data, an analysis of the pressure drop induced by the turbine, the thermodynamics of the air–water vapour mixture compression process and its deviations from the expected ideal gas performance has been carried out. As this way, we expect to learn how the process evolves from the initial to final states and the extent of influence of moisture.

The pressure drop Δp between the chamber inner and leeward side of the turbine is plotted versus the experimental outflow temperature $T_{2\,exp}$ in figure 12, for the two moisture conditions imposed. Values up to 500 Pa of pressure drop indicate that the experimental set up provides a more efficient performance, when compared with the more simplified set up used in the first experiments, [49]. In order to achieve a better understanding of the compression process undergone by the system from the state (T_1, p_1) in the plenum region, values of temperature as predicted under the hypothesis of adiabatic process of both ideal and real gas (noted as $T_{2\,ad}$ and $T_{2\,adZ}$ respectively), and under the conservation of mass flow and enthalpy in a real gas system (noted as T_2) are considered.

First, the final state temperature $T_{2\,ad}$ as a result of an adiabatic process of an ideal gas described as:

$$p v_m^{\gamma} = const \tag{37}$$

is calculated after combination of (37) with the state equation of the ideal gas (16):

$$T_{2\,ad} = T_1 \left(\frac{p_2}{p_1}\right)^{\frac{\gamma-1}{\gamma}} \tag{38}$$

where (T_1, p_1, p_2) are the experimental values of temperature and pressure, and $\gamma \simeq 1.4$ for air considered as an ideal system.

Second, the final state temperature $T_{2\,adZ}$ under the hypothesis of adiabatic process in a real gas system, is calculated for the same set (T_1, p_1, p_2) by means of the process equation:

$$p v_m^n = const \tag{39}$$

which implies $n = ZC_p/C_V$ as deduced in previous sections. Therefore, combining (39) and the state equation of the real gas (19):

$$T_{2\,adZ} = T_1 \left(\frac{Z_1}{Z_2}\right)\left(\frac{p_2}{p_1}\right)^{\frac{n-1}{n}} \tag{40}$$

Third, the temperature T_2 required for the conservation of mass flow and enthalpy is deduced based on the real gas formulation according to the methodology detailed in Medina–López *et al.* [49], in which no specific requirement related to the adiabatic nature of the process is included. Indeed, the value of T_2 is calculated numerically iterating the expression (34) of the outflow velocity U_2 once the values of h_1 and C_{p2} are calculated from the experimental data (T_1, p_1, p_2) alongside with the state functions (28) and (30) for the real gas, and the mass flow conservation condition.

The scheme in figure 12 reveals two essential aspects of the air–water vapour mixture compression process so far, which in turn are coupled through the thermodynamic variables: the extent to which the process can be considered strictly adiabatic, and the role of moisture in the nature of the system for its consideration as a real gas. In relation to the implications of the adiabatic nature of the process, in the case of higher moisture the values T_2 calculated from the conservation of enthalpy and mass flow are the ones which match best the experimental values of temperature $T_{2\,exp}$ in the final state. As it has been stated previously, those values implement the real gas model but with no additional hypothesis on the characteristics of the process itself. In addition, there are noticeable differences between experimental values $T_{2\,exp}$ and the values calculated with the adiabatic process hypothesis, regardless of the system be considered as ideal gas —$T_{2\,ad}$ values from (38)— or real gas —$T_{2\,adZ}$ values from (40)—. Anyway, there is a good fit for the lowest pressure drops —i. e. $\Delta p \lesssim 100\,Pa$— for both higher and lower moisture values. On the other hand, there is a tendency in the system to behave more as an ideal gas for the lower water vapour concentration, as it can be deduced from the similarity between $T_{2\,ad}$, $T_{2\,adZ}$ and T_2, but again the process differs from the adiabatic condition as its revealed by the differences with $T_{2\,exp}$.

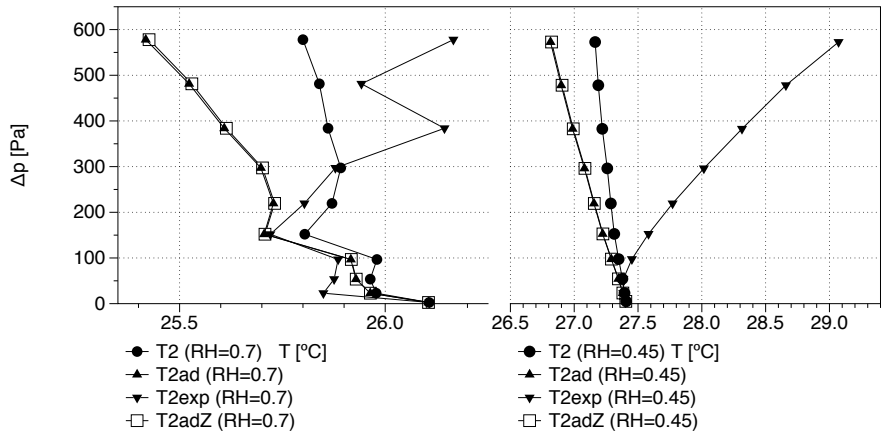

Figure 12: Pressure drop for stationary flow for high (left) and low (right) air moisture conditions.

From the above discussion, it can be concluded that for the higher values of pressure drop, an increase in the water vapour concentration modifies the thermodynamic nature of the system so that it behaves as a real gas system following

a process which is not entirely adiabatic, conversely to what it could be initially supposed. Nonetheless, for the lowest values of pressure drop the system can be considered as an ideal gas bound to an adiabatic process.

4.2. Polytropic exponent n for the real gas

A description of the characteristics of the compression process of the real gas meeting the conservation of enthalpy and mass flow, and under conditions different from adiabatic, can be reached through the general process equation and the polytropic exponent n. To this end, let us recall again that a general expression for the temperature in a general process, not necessary adiabatic, of a real gas system, can be deduced combining the process equation (1) and the state equation (19) for the real gas:

$$T_2 = T_1 \left(\frac{Z_1}{Z_2}\right) \left(\frac{p_2}{p_1}\right)^{\frac{n-1}{n}} \tag{41}$$

where now n remains undefined —up to this point, if $n = ZC_p/C_V$ it would be assumed that the process is adiabatic—. The expression (41) can be used to determine which values of n are required for the process so that the final state temperature values be equal to the values T_2 deduced through the conservation of enthalpy. When solving (40) for the known values (T_1, p_1, Z_1) and (T_2, p_2, Z_2), the new values of n for the two moisture conditions differ from the values of a standard adiabatic process, i. e. $n \equiv \gamma = 1.4$ for air as an ideal gas or $n = 1.67$ for an ideal monoatomic gas. The results are represented in figure 13 versus the non dimensional temperature $T^* = T_2/T_1$ for each water vapour concentration.

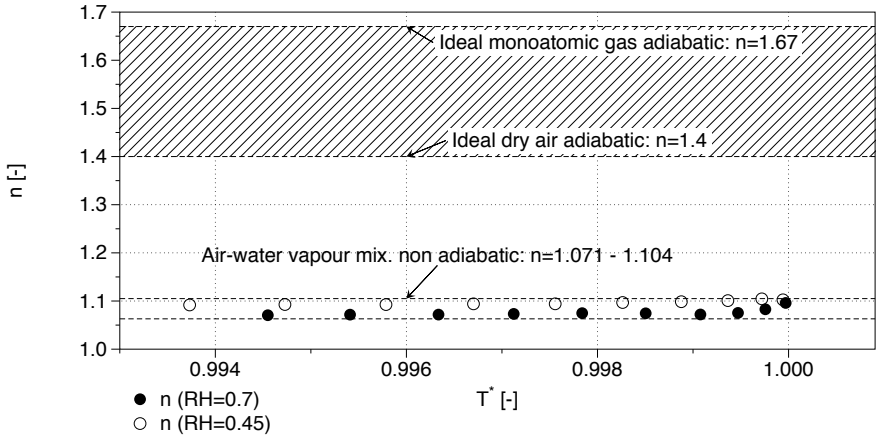

Figure 13: Polytropic exponent n for the compression process vs. non dimensional temperature $T^* = T_2/T_1$.

For the higher water vapour concentration $n \simeq 1.071$ on average while for the lower concentration $n \simeq 1.104$, showing an increasing trend as T^* increases. Actually, it is clear from the previous rationale that n represent the implicit dependence of the process with the second virial coefficient B as a function of temperature, through the compressibility factors Z_1 and Z_2 in the initial and final states respectively. So it seems reasonable to expect an increasing trend of n with temperature as it is for B, specially for the lower range of temperatures, figure 3. Moreover, the behaviour of the compression process as described by the polytropic exponent n represented in figure 13 seems to be consistent with the results plotted in figure 12. The effect of water vapour is to modify the system nature in the direction of a real gas system which in turn is not following a totally adiabatic process. Hence the higher the water vapour concentration, the more the shifting away from the ideal gas adiabatic process conditions. In that sense, as the moisture concentration increases the n moves away from the expected value $n = 1.4$ in the case of adiabatic air or $n = 1.67$ in the case of adiabatic monoatomic system. In fact, the results are in agreement with values observed in thermodynamic processes of simple closed systems in which the adiabatic condition is not totally fulfilled, [62].

The experimental values $T_{2\,exp}$ show differences with the values T_2 as deduced form the conservation of enthalpy, the more noticeable as the water vapour concentration decreases. This could be explained in terms of some missing control in the temperature variable at the outflow section due to difficulties in the placement of the temperature probe —in contrast with the pressure gauges—, to the turbulence and swirl in the flow jet leeward of the turbine orifice and to heat exchange with the surroundings. In consequence, the point to measure the exit temperature might not be entirely suitable to observe a thermodynamic property as representative of a process in a closed system, but only a part of it which cannot be regarded as closed.

4.3. Effects on pressure drop and power input

The effects of moisture on the OWC performance can be viewed through the analysis of the pressure drop through the turbine. Non dimensional variables are used in order to generalize results.

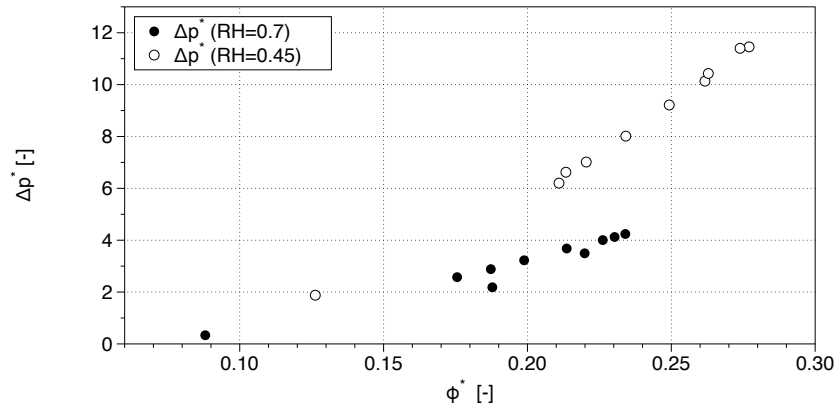

Figure 14: Non dimensional flow vs. pressure drop for both high and low moisture conditions.

The figure 14 represents the non dimensional pressure drop Δp^* as a function of the non dimensiona flow discharge ϕ^* for the two moisture conditions observed. Following [49], Δp^* is calculated in the form:

$$\Delta p^* = \frac{\Delta p}{\rho_1 w^2} \left(\frac{1 - RH_1}{RH_1} \right) \tag{42}$$

where Δp is the pressure drop as calculated from the experimental dataset, ρ_1 is the air density of the air–water vapour mixture at the turbine inlet, w represents the air velocity relative to the turbine, and RH_1 relative humidity in the region windward the turbine. It is deduced from the results that the water vapour concentration does not concern essentially the linear performance of the turbine. However, while for discharge values $\phi^* \leq 0.15$ the pressure drop is basically independent of the water vapour concentration, for higher values the pressure drop is reduced up to 30 % as the relative humidity is increased from 0.4 to 0.7. The reduction has a direct impact on the available pneumatic power, calculated as $W_{pneu} = \Delta pQ$, and in the hydrodynamic efficiency, calculated as the ratio between pneumatic power and impinging wave power.

It is important to highlight that while this result is consistent with experiments previously conducted by the authors, [49], it has been included here for self–consistence and replicability according to the new experimental set up.

With the objective of evaluating quantitatively the importance of that results, a numerical example based on a real plant is devoted for the purpose. Let us consider the OWC power plant of Pico (Azores) and its configuration (see for example [63], [64]). The chamber geometry is defined by a square floor of $12 \times 12\, m^2$ with an inner volume of $V_{owc} = 1050\, m^3$ above the free water surface. The turbine with a $D_t = 2.3\, m$ exterior diameter is described by a turbine characteristic number of $K = 0.6803$ and a maximum rotation velocity of $N = 1500\, rpm\, (157,1\, rad/s)$. Given a sea state with significant wave height of, say, $H_s = 2\, m$ and peak period $T_p = 11\, s$, the non-dimensional flow through the turbine would reach a maximum value of $\phi^* = 0.0494$, assuming a capture length value of approximately 0.7 following [15]. Now, being the air density of $\rho_a = 1.204\, kg/m^3$ and the reference pressure $p_{atm} = 101325\, Pa$, if the dimensionless pressure drop, Δp^*, is calculated by both the classical formulation (adiabatic process with $n = \gamma = 1.4$) and the real gas formulation with a polytropic exponent for a 70 % of moisture ($n = 1.071$), the values of 0.0719 and 0.0630 respectively are obtained. According to the hypotheses previously introduced, in terms of dimensionless power output ($\Pi^* = \Phi^* \cdot \Delta p^*$), the values of 0.0036 and 0.0031 respectively are calculated. This results suggests that the consideration of the real gas formulation helps to explain a reduction of non-dimensional power output of 12.4 % compared with the calculated by the classical formulation.

In order to provide a clear view of the real gas model in the estimation of non-dimensional power output in OWC devices, the figure 15 shows the difference between dimensionless power output in Pico Plant case study for several typified sea states $(H_s; T_p) = (\{0.5; 5\}, \{1.0; 7\}, \{2.0; 11\}, \{3.0; 13\}, \{4.0; 15\})$. An increase in the difference of non-dimensional power output from both models when the dimensionless flow through the turbine increases is appreciated. In addition, the non-dimensional power output is lower for the real gas model than the ideal model in all cases.

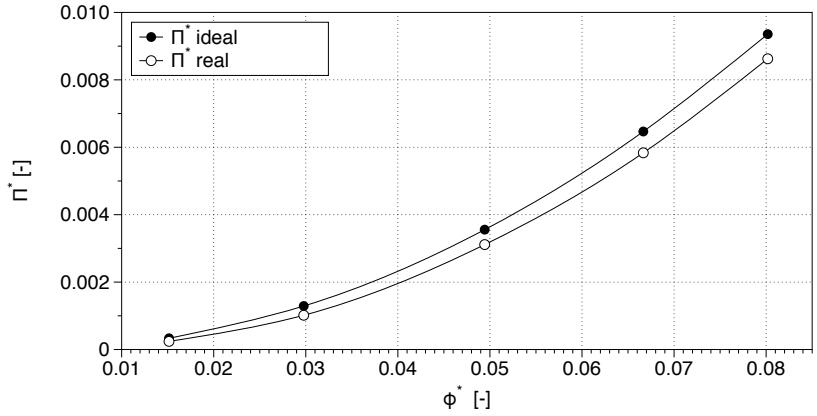

Figure 15: Non dimensional flow vs. non dimensional power output in Pico Plant case study for both the real gas model and the classical theory in several sea states.

It is necessary to emphasize that although the dimensionless flow of the experimental set up studied is of the same order of magnitude as that obtained for the Pico plant, the non-dimensional pressure drop are not comparable since the turbine typology used differs in both cases.

Finally, following the research in [57], there might be present scale effects in a full scale prototypes such as the one considered in the previous example, and it requires a deeply focused study. The non-uniformities in the air system variables distribution would lead to transient non-equilibrium states, otherwise not observed at small scales. Those transient states, in turn, would force a momentary deviation from the closed system performance. From a qualitative point of view and considering a wave cycle as a time reference, that would probably induce a sequence of in-between system states in which pressure and temperature would not reach the corresponding polytropic states. While the effects could be more or less negligible when dealing with full scale prototypes designed for extreme wave climate conditions, there might be differences in the long-term management fo devices designed for mild wave climate conditions, as focused in the ongoing research underlying the present work.

5. Conclusions and future research

It has been studied the behaviour of the air–water vapour mixture, forced to compression in a simple OWC chamber model under the consideration of a real gas model. The nature of the thermodynamic process has been studied by means of the polytropic exponent defining the compression process. While the experiments are conducted under stationary flow, the thermodynamic compression process undergone by the control volume system allows a better focusing on the main features without loss of generalization. The major findings in this research are:

1. The air–water vapour mixture behave as a real gas undergoing a not entirely adiabatic process for higher values of moisture, i. e. $RH \gtrsim 70\,\%$. The final state temperature T_2 fits better the experimental observations when the real gas formalism is implemented in the conservation of enthalpy and mass flow under no specific constraints regarding adiabaticity.
2. For lower water vapour concentration, the air–water vapour system tends to behave as an ideal gas, as it is revealed by the simmilarities between T_{2ad}, T_{2adZ} and T_2. However, the small differences with the experimental results, around $0.3\,\%$ in average, seems to indicate that the process slightly deviates from the adiabatic condition. That situation is coherent with the deviation of index n from its adiabatic values, see figure 13.
3. For the lower range of pressure drops, i. e. $\Delta p \lesssim 100\,Pa$, the distinction between ideal and real gas hypothesis become less relevant and the differences in the final state temperature are reduced.
4. The polytropic exponent n is re–calculated, so that the state (T_2, p_2) can be obtained from (T_1, p_1) preserving enthalpy. The values indicate that the polytropic exponent ranges between $n \simeq 1.071$ for higher moisture values and $n \simeq 1.104$ for lower moisture, in a similar way to the performance observed by other authors, [62]. Those values bring to front that neither the process is totally adiabatic, nor the system can be described as an ideal gas. The expected value of n for an ideal gas system undergoing an adiabatic process should be $n = C_p/C_V$, taking a value 1.67 in the case of a monoatomic gas or 1.4 in the case of air. While the experiments are run with air, the differences with the expected value providing with a new focusing on the nature of the system and the thermodynamic process.

5. In terms of pressure drop and available power, the results of the experimental set up suggest that the increase in moisture between 45% and 70% in the air–water vapour mixture induces reductions in the power input to the turbine around 30%. Now, the values of the polytropic exponent allow to implement in the formulation of the problem, even as a rough estimate, the realistic hypothesis of a not entirely adiabatic process in the radiation–diffraction classical approach. In fact, for the well known power plant of Pico, it is possible to advice a reduction of dimensionless power input of 12.4% between the classical and the real gas formulation. From that point on, it is feasible to achieve a better theoretical description directly oriented to technical investment and long–term management.
6. The scale effects is one of the next steps to take, as the natural evolution of the research line presented in this work is to increase the size and configuration of test models. The study of the scale effects will help in a better understanding and management of the OWC efficiency based on the previous results.

From this point, the next step in the research is to test an OWC chamber in a wave tank, so that the analysis of data can be used to verify the real gas performance under oscillatory flow conditions. With that new approach in terms of thermodynamic behaviour and its transposition to the efficiency finally achieved, a better knowledge can be achieved to adjust production, equipment and maintenance costs throughout the device lifespan. Those adjustments are considered essential for the management of scientific and technological efforts towards a competitive, simple and easily replaceable and/or repairable OWC solutions.

References

[1] Soytas U. & Sari R., 2003. *Energy consumption and GDP: causality relationship in G-7 countries and emerging markets.* Energy Economics, Vol.25, Nª 1, pp. 33–37.

[2] Antonakakis N., Chatziantoniou I. & Filis G., 2017. *Energy Consumption, CO2 Emissions, and Economic Growth: A Moral Dilemma.* MPRA Paper 67422, University Library of Munich, Germany.

[3] World Energy Council, 2016. *World Energy Resources 2016.* World Energy Council. 1028 p.p.i.s.b.n. 978 − 0 − 946121 − 58 − 8.

[4] Boake C. B., Whittaker T. J. T., Folley M. & Ellen H., 2002. *Overview and Initial Operational Experience of the LIMPET Wave Energy Plant.* Proceedings of The 12th International Offshore and Polar Engineering Conference, pp. 586–594.

[5] Torre-Enciso Y., Ortubia I., López de Aguilera L. I. & Marqués J., 2009. *Mutriku Wave Power Plant: from the thinking out to the reality.* 8th European Wave and Tidal Energy Conference (EWTEC 2009). pp. 319–328.

[6] Uihlein A. & Magagna D., 2015. *Wave and tidal current energy - A review of the current state of research beyond technology.* Renewable and Sustainable Energy Reviews, Vol. 58, pp. 1070–1081.

[7] Bahaj A., 2011. *Generating electricity from the oceans.* Renewable and Sustainable Energy Reviews, Vol.15, Nº 7, pp. 3399–3416, DOI 10.1016/j.rser.2011.04.032.

[8] IEA, 2016. *World Energy Outlook 2016.* International Energy Agency, pp. 684.

[9] O'Hagan A.M., Huertas C., O'Callaghan J. & Greaves D., 2016. *Wave energy in Europe: Views on experiences and progress to date.* International Journal of Marine Energy, Vol.14, pp. 180–197.

[10] Falcão A. F. de O., 2010. *Wave Energy Utilization: A Review of the Technologies.* Renewable and Sustainable Energy Reviews, Vol. 14, Issue. 3, pp. 899–918.

[11] SI Ocean, 2012. *Ocean energy: State of the Art.* Strategic Initiative for Ocean Energy (SI Ocean) Tech. Report, Brussels (Belgium), pp. 78.

[12] López I., Andreu J., Ceballos S., Martínez de Alegría I. & Kortabarria I., 2013. *Review of Wave Energy Technologies and the Necessary Power-Equipment.* Renewable and Sustainable Energy Reviews, Vol. 27, pp. 413–434.

[13] The Carbon Trust, 2005. *Oscillating Water Column Wave Energy Converter Evaluation Report.* Marine Energy Challenge, pp. 196.

[14] Raghunathan S., 1995. *The Wells Turbine for Wave Energy Conversion.* Prog. Aerospace. Sci., Vol. 31, pp. 335–386.

[15] Martins–Rivas H. & Mei C. C., 2009. *Wave Power Extraction from an Oscillating Water Column at the Tip of a Breakwater.* Journal of Fluid Mechanics, Vol. 626, pp. 395–414.

[16] Martins–Rivas H. & Mei C. C., 2009. *Wave Power Extraction from an Oscillating Water Column along a Straight Coast.* Ocean Engineering, Vol. 36, pp. 426–433.

[17] Rezanejad, K., Bhattacharjee, J. & Guedes–Soares C., 2013. *Stepped sea bottom effects on the efficiency of nearshore oscillating water column device.* Ocean Engineering, Vol. 70, pp. 25–38.

[18] Medina–López E., Bergillos R. J., Moñino A., Clavero M. & Ortega–Sánchez M., 2017. *Effects of Seabed Morphology on Oscillating Water Column Wave Energy Converters.* Energy, Vol. 135, pp. 659–673.

[19] Bergillos R. J., López-Ruiz A., Medina-López E., Moñino A. & Ortega-Sánchez C., 2018. *The role of wave energy converter farms on coastal protection in eroding deltas, Guadalfeo, southern Spain.* Journal of Cleaner Production, Vol. 171, pp. 356–367.

[20] Korde U., 1991 *A Power Take–Off Mechanism for Maximizing the Performance of an Oscillating Water Column Wave Energy Device.* Applied Ocean Research, Vol. 13, pp. 75–81.

[21] Falcão A. F. de O. & Justino P. A. P., 1999. *OWC Wave Energy Devices with Air Flow Control*. Ocean Engineering, Vol. 26, pp. 1275–1295.
[22] Falcão A. F. de O., 2008. *Phase Control through Load Control of Oscillating Body Wave Energy Converters with Hydraulic PTO System*. Ocean Engineering, Vol. 35, pp. 358–366.
[23] Gomes R. P. F., Henriques J. C. C., Gato L. M. C. & Falcão A. F. de O., 2014. *Hydrodynamic optimization of an axisymmetric floating oscillating water column for wave energy conversion*. Renewable Energy, Vol. 44, pp. 328–339.
[24] Shaaban S., 2016. *Aero-economical optimization of Wells turbine rotor geometry*. Energy Conversion and Management, Vol. 126, pp. 20–31.
[25] Gkikas G. D. & Athanassoulis D. A., 2014. *Development of a Novel Nonlinear System Identification Scheme for the Pressure Fluctuation inside an Oscillating Water Column Wave Energy Converter Part I: Theoretical Background and Harmonic Excitation Case*. Ocean Engineering, Vol. 80, pp. 84–99.
[26] López-Ruiz. A., Solari S., Ortega-Sánchez M. & Losada M., 2015. *A simple approximation for wave refraction - Application to the assessment of the nearshore wave directionality*. Ocean Modelling, Vol. 96, pp. 324–333.
[27] Halder P. & Samad A., 2016. *Optimal Wells turbine speeds at different wave conditions.*International Journal of Marine Energy, Vol. 16, pp. 133–149.
[28] Falcão A. F. de O. & Rodrigues R. J. A., 2002. *Stochastic modelling of OWC wave power plant performance*. Applied Ocean Research, Vol. 24, Nº 2, pp. 59–71.
[29] López. I., Pereiras B., Castro F. & Iglesias G., 2014. *Optimisation of Turbine-Induced Damping for an OWC Wave Energy Converter using a RANS-VOF Numerical Model*. Applied Energy, Vol. 127, pp. 105–114.
[30] Iturrioz A., Guanche R., Lara J. L., Vidal C. & Losada I. J., 2015. *Validation of OpenFOAM® for Oscillating Water Column three-dimensional modeling.*Ocean Engineering, Vol. 107, pp. 222–236.
[31] Moñino A., Medina-López E., Clavero M. & Benslimane S., 2017. *Numerical simulation of a simple OWC problem for turbine performance*. International Journal of Marine Energy, 20, pp. 17–32.
[32] Carballo R., Sánchez M., Ramos V., Fraguela J. A. & Iglesias G., 2015. *The intra-annual variability in the performance of wave energy converters: A comparative study in N Galicia (Spain)*. Energy, 82, pp. 138–146.
[33] Jalón L., María L., Baquerizo A. & Losada M. A., 2016. *Optimization at different time scales for the design and management of an oscillating water column system.*Energy, Vol. 95, pp. 110–123.
[34] Lin L. & Yu H., 2012. *Offshore wave energy generation devices: Impacts on ocean bio-environment*. Acta Ecologica Sinica, Vol. 32, pp. 117–122.
[35] Heras-Saizarbitoria I., Zamanillo I. & Laskurain I., 2013. *Social acceptance of ocean wave energy: A case study of an OWC shoreline plant*. Renewable and Sustainable Energy Reviews, Vol. 27, pp. 515–524.
[36] Crooks D., Andres A. De & Medina-Lopez E., 2017. *Demonstration of a Socio-economic Cost of Energy Analysis of a Wave Energy Converter Array*. Conference Paper, pp. 1–12.
[37] Evans D. V., 1982. *Wave Power Absorption by Systems of Oscillating Pressure Distributions*. Journal of Fluid Mechanics, Vol. 114, pp. 481–499.
[38] Sarmento A. J. N. A. & Falcão A. F. de O., 1985. *Wave Generation by an Oscillating Surface–Pressure and its Application in Wave–Energy Extraction*. Journal of Fluid Mechanics, Vol. 150, pp. 467–485.
[39] Mei C. C., 1989. *The Applied Dynamics of Ocean Surface Waves*. World Scientific. 740 p.p. i.s.b.n. 9971 − 50 − 789 − 7.
[40] Falnes J., 2007. *A review of wave-energy extraction*. Marine Structures, Vol. 20, Nº 4, pp. 185–201.
[41] Nader J. R., Zhu S. P., Cooper P. & Stappenbelt B., 2012. *A finite-element study of the efficiency of arrays of oscillating water column wave energy converters*. Ocean Engineering, Vol. 43, pp. 72–81.
[42] Lovas S., Mei C. & Liu Y., 2010. *Oscillating Water Column at a Coastal Corner for Wave Power Extraction*. Applied Ocean Research, Vol. 32, pp. 267–283.
[43] Medina–López E., Moñino A., Bergillos R. J., Clavero M. & Ortega–Sánchez M., 2019. *Oscillating Water Column Performance under the Influence of Storm Development*. Energy, 166, pp. 765–774.
[44] Sheng W., Alcorn R., & Lewis S., 2013. *On Thermodynamics of Primary Energy Conversion of OWC Wave Energy Converters*. Renewable Sustainable Energy, 5, 023105.
[45] Kim T. S., Song C. H., Ro S. T. & Kauh S. K., 1991 *Influence of ambient condition on thermodynamic performance of the humid air turbine cycle*. Energy, Vol. 4, Nº4, pp. 313–324.
[46] Rahman M.M., Ibrahim-Thamir K., Kadirgama K., Mamat R. & Bakar-Rosli A., 1995. *Influence of Operation Conditions and Ambient Temperature on Performance of Gas Turbine.*Advanced Materials Research, Vol. 189–193, pp. 3007–3013.
[47] Yang W. & Su M., 2004. *Influence of Moist Combustion Gas on Performance of a Sub-Critical Turbine*. Energy Conversion & Management Vol. 46, pp. 821–832.
[48] Singh S. & Kumar R., 2012. *Ambient Air Temeprature Effect on Power Plant Performance*. International Journal of Engineering Science & Technology, Vol. 4, Nª 8, pp. 3916–3928.
[49] Medina–López E., Moñino A., Clavero M., Del Pino C. & Losada M. A., 2016. *Note on a Real Gas Model for OWC Performance*. Renewable Energy, Vol. 85, pp. 588–597.
[50] Medina–López E., Moñino A., Borthwick A. G. L. & Clavero M., 2017. *Thermodynamics of an OWC Containing Real Gas*. Energy, Vol. 135, pp. 709–717.
[51] Medina–López E., Borthwick A. & Moñino A., 2019. *Analytical and Numerical Simulations of an Oscillating Water Column with Humidity in the Air Chamber*. Journal of Cleaner Production, Vol. 238, 117898.

[52] Prausnitz J., Lichtenthaler R. & Gomes de Azevedo E., 1999. *Molecular Thermodynamics of Fluid–Phase Equilibria.* Prentice–Hall. 864 pp. i.s.b.n. $0-13-977745-8$

[53] Malic D., 1955. *The Equation of Polytropic Process of Real Gas.* journal of the Franklin Institute, Vol. 259, Issue 3, pp. 235–238.

[54] Pitzer K. S. & Curl R.F., 1957. *The Volumetric and Thermodynamic Proterties of Fluids. III. Empirical Equation for the Second Virial Coefficient.* Thermodynamic Properties of Fluids, Vol.79, pp. 2369–2370.

[55] Gel'man L. I. & Smolkin Y. V., 1966. *On the Calculation of Adiabatic Processes in Real Gases.* Journal of Engineering Physics, Vol. 11, Nª 33, pp. 325–328.

[56] Wisniak J., 2003. *Heike Kamerlingh – The Virial Equation of State.* Indian Journal of Chemical Technology, Vol. 10, pp. 564–572.

[57] Dimakopoulos A., Cooker M. J., & Bruce T., 2017. *The Influence of sScale on the Air Flow and Pressure in the Modelling of Oscillating Water Column Wave Energy Converters.* International Journal of Marine Energy, Vol. 19, pp. 272–291.

[58] Biel Gayé, J., 1986. *Formalismo y Método de la Termodinámica. Teoría General, Aplicaicones y Ejercicios Resueltos.* Apuntes de clase. Universidad de Granada, 258 pp.

[59] Landau L., Ajiezer A. & Lifshitz E., 1988. *Curso de Física General. Mecánica y Física Molecular.* 3ª reimpresión. MIR. 398 p.p.

[60] Tsonopoulos C. & Heidman J. L., 1990. *From the Virial to the Cubic Equation of State.* Fluid Phase Equilibria, Vol. 57, pp. 261–276.

[61] Bell J. H. & Mehta R. D., 1988. *Contraction Design for Small Low–Speed Wind Tunnels.* Report JIAA TR–84. Joint Institute for Aeronautics and Acoustics, National Aeronautics and space Administration, Stanford University.

[62] Prisnyakov V. F., 1967. *Calculaiton of the Process of Filling a Gas Container.* Vol. 13, Nº 3, pp. 367–372.

[63] Justino P.A.P. & Falcão A. F. de O., 1999. *Rotational Speed Control of an OWC Wave Power Plant.*Journal of Offshore Mechanics and Arctic Engineering, Vol. 121, pp. 65–70.

[64] Falcão A. F. de O., 2002. *Control of an oscillating-water-column wave power plant for maximum energy production.* Applied Ocean Research, Vol. 24, pp. 73–82.

List of Figures

List of Symbols

A_t—Turbine cross section area — $[m^2]$
A_b—Turbine blades area — $[m^2]$
B—Second virial coefficient
C—Third virial coefficient
C_p—Specific heat under constant pressure — $[J/mol \cdot K]$
C_p^*—Specific heat under constant pressure for the ideal gas — $[J/mol \cdot K]$
C_V—Specific heat under constant pressure $[J/mol \cdot K]$
C_V^*—Specific heat under constant pressure for the ideal gas — $[J/mol \cdot K]$
C_y—Specific heat under constant state equation y — $[J/mol \cdot K]$

D_{owc}—OWC diameter — $[m]$
D_t—Turbine diameter — $[m]$
f_0, f_1, f_2—Temperature correlation functions — $[-]$
g—Gravity acceleration — $[m^2/s]$
h—Specific enthalpy — $[J/kg]$
h^*—Specific enthalpy for the ideal gas — $[J/kg]$
H_s—Significant wave height — $[m]$
H_i, H_e—Contraction height from centerline at inlet/exit sections — $[m]$
K—Turbine characteristic number — $[m]$
K_t—Isothermal compressibility coefficient —$[1/Pa]$
L—Plenum contraction length — $[m]$
m—Polytropic index —$[-]$
m_a—Mass of dry air — $[kg]$
m_v—Mass of water vapour — $[kg]$
MW_a–Molar weight of air — $[kg/mol]$
MW_v—Molar weight of water vapour — $[kg/mol]$
n—Polytropic exponent —$[-]$
N—Number of moles $[mol]$ or Turbine rotation velocity $[rad/s]$
p—Pressure — $[Pa]$
$p_{atm} = 101325\,Pa$—Atmospheric pressure
p_1, p_2—Experimental pressure at inflow/outflow sections — $[Pa]$
$p_c = 2.2089 \cdot 10^7\,Pa$—Critical pressure of water
p_r—Reduced pressure, $p_r = p/p_c$ — $[-]$
Q_{owc}—Volumetric flow rate at the turbine inlet
$R_a = 286.7\,J/K \cdot kg$—Dry air constant
$R_v = 461.0\,J/K \cdot kg$—Water vapour constant
R_{owc}—OWC radius
$R_0 = 8.31\,J/K \cdot mol$—Universal gas constant
RH—Relative humidity
$s = S/N$—Unitary entropy — $[J/mol \cdot K]$
T—Temperature — $[K]$
T^*—Dimensionless temperature — [-]
$T_c = 647\,K$—Critical temperature of water
T_p— Wave peak period — $[s]$
T_r—Reduced temperature, $T_r = T/T_c$ — $[-]$
$T_1, T_{2\,exp}$—Experimental temperature at inflow/outflow sections — $[K]$
T_2—Temperature of real gas for conservation of enthalpy at outflow section — $[K]$
$T_{2\,ad}$—Temperature for adiabatic process of ideal gas att outflow section — $[K]$
$T_{2\,adZ}$—Temperature for adiabatic process of real gas at outflow section— $[K]$
U—Flow velocity along turbine axis direction — $[m/s]$
U_t—Blade circumferential velocity at balde tip — $[m/s]$
$v_m = V/N$—Molar volume of gas — $[m^3/mol]$
V_{owc}—Air volume inside the chamber
w—Air velocity relative to the turbine
W_{pnew}— Pneumatic work — $[J]$
x— Auxiliary variable
y— Auxiliary variable
Z—Compressibility factor — $[-]$

Greek

α—Isobaric expansion coefficient — $[-]$
Δp—Pressure drop through the turbine — $[Pa]$
Δp^*—Non dimensional pressure drop through the turbine — $[-]$
$\gamma = 1.4$—Heat capacity ratio for air (ideal gas) — $[-]$
$\gamma = 1.67$—Heat capacity ratio for monoatomic gas (ideal gas) — $[-]$
Π^*—Non dimensional power output — $[-]$
ρ—Density — $[kg/m^3]$
σ—Turbine solidity — $[-]$
$\Phi^* = U/U_t$—Non dimensional discharge through the turbine — $[-]$
χ_{mol}—Molar fraction of vapour in dry air
ω—Acentric factor — $[-]$